JOURNAL OF GEOPHYSICAL RESEARCH, VOL. 114, C01015, doi:10.1029/2008JC005077, 2009

An experimental study of spatial evolution of statistical parameters in a unidirectional narrow-banded random wavefield

Lev Shemer[1] and Anna Sergeeva[2]

Received 11 August 2008; revised 24 September 2008; accepted 7 October 2008; published 29 January 2009.

[1] Unidirectional random waves generated by a wavemaker in a 300-m-long wave tank are investigated experimentally. Spatial evolution of numerous statistical wavefield parameters is studied. Three series of experiments are carried out for different values of the nonlinear parameter ε. It is found that the frequency spectrum of the wavefield undergoes significant variation in the course of the wavefield evolution along the tank. The initially narrow Gaussian spectrum becomes wider at the early stages of the evolution and then narrower again, although it still remains wider than the initial spectrum at the most distant measuring location. It is found that the values of all the statistical wave parameters are strongly related to the local spectral width. The deviations of various statistical parameters from the Gaussian statistics increase with the width of the spectrum so that the probability of extremely large (the so-called freak) waves is highest when the local spectral width attains maximum. The deviations from the Rayleigh distribution also become more pronounced when the nonlinearity parameter ε is higher. It is found that the Tayfun and Fedele 3rd order random wavefield model provides an appropriate description of the observed phenomena. An attempt is made to relate the spatial variations of the wavefield statistics reported here to the wavefield recurrence, as suggested recently.

Citation: Shemer, L., and A. Sergeeva (2009), An experimental study of spatial evolution of statistical parameters in a unidirectional narrow-banded random wavefield, *J. Geophys. Res.*, *114*, C01015, doi:10.1029/2008JC005077.

1. Introduction

[2] Nonlinear interactions of ocean waves are usually stochastic in nature. A large number of harmonics with various frequencies exchange energy and transfer it to shorter scales at which wave energy is dissipated by breaking or otherwise. This phenomenon is sometimes called "wave" or "weak", turbulence, to acknowledge similarity to Kolmogorov energy cascade in fluid turbulence. *Hasselmann* [1962] was the first to apply statistical approach and the kinetic theory to describe ocean wave turbulence. Recently water wave turbulence theory was advanced considerably by Zakharov and his colleagues [see, e.g., *Zakharov*, 1999, and references therein]. The kinetic wave theory serves as a basis for modern wave climate prediction. The kinetic theory of random ocean waves is based on two fundamental assumptions: weak nonlinearity of waves and randomness of their phases. The random phase approximation is an essential assumption used for turbulent closures for all stochastic wave systems and even for a much broader range of turbulent systems.

[3] Numerous attempts have been made to explore the possibility to use deterministic nonlinear wave theories to forecast the evolution of a random wavefield [see, e.g., *Stiassnie and Shemer*, 2005; *Annenkov and Shrira*, 2006a, 2006b; *Onorato et al.*, 2007]. These studies reveal the crucial role of nonresonant interactions in the evolution of nonlinear random water waves. This understanding makes the experiments in a wave tank, where nontrivial exact resonances do not exist since only near-resonant interactions between unidirectional waves are possible, a very convenient vehicle to study nonlinear random waves in laboratory conditions. Some experiments in a long wave tank have recently been performed on deep narrow-banded waves with random phases [*Mori et al.*, 2007, and references therein]. Results of these experiments indicate that in spite of lack of exact resonances in a unidirectional wavefield, nonlinear effects are essential and they strongly affect the statistical properties of the wavefield. Similar conclusions were reached in a numerical study of shallow-water random wavefields modeled by *Pelinovsky and Sergeeva* [2006] using the Korteweg-de Vries equation.

[4] Theoretical investigations aimed at describing the statistical properties of nonlinear wavefields were originated by *Longuet-Higgins* [1952] who showed that for a narrow-banded wavefield with random phases, wave heights satisfy the Rayleigh distribution. An improved model that takes into account nonlinear effects has been suggested later by *Longuet-Higgins* [1963]. More recently, numerous models appropriate to unidirectional wavefields were proposed [*Naess*, 1985; *Tayfun*, 1980, 2006; *Tayfun and Fedele*, 2007, and references therein]. In particular, these models were applied to address the problem of unusually steep (the so-called freak, or rogue) waves of considerable interest.

[1]School of Mechanical Engineering, Tel-Aviv University, Tel-Aviv, Israel.

[2]Institute of Applied Physics, Russian Academy of Sciences, Nizhny Novgorod, Russia.

0148-0227/09/2008JC005077$09.00

Such waves, often dubbed killer waves, appear and disappear fast and unexpectedly, and have the potential of causing substantial damage to marine traffic. The relatively high occurrence of those waves that exceeds the predictions based on the Rayleigh distribution suggests that the occurrence of freak waves is related to nonlinearity of the wavefield. Mechanisms leading to freak wave appearance, as well as the determination of their probability for a given sea state are thus not only of practical importance, but they also demand in depth study using the most advanced theoretical approaches and laboratory experiments.

[5] In the present study we carry out an experimental investigation of the evolution of a random wavefield in a large wave tank. Variations along the tank of various statistical properties of the wavefield of relevance to appearance of freak waves are investigated. The contribution of nonlinear effects to deviations of the wave statistics from the Rayleigh distribution is demonstrated. In particular, the spatial evolution of wave spectra is considered. The spectral shape varies noticeably along the tank due to the nonlinearity of the wavefield. The spectral widening is related to the variation of the high-order statistical moments of the surface elevation, and of the probability distribution functions of wave heights, crests and troughs.

2. Experimental Facility and Procedure

[6] The experiments were carried out in the Large Wave Channel (GWK) in Hanover, which is about 300 m long, 5.0 m wide and 7.0 m deep. The water depth in the present experiments was set at h = 5 m. A sand beach with a slope of 30° is located at the far end of the facility, starting at x = 270 m. The computer-controlled piston-type wavemaker is equipped with a system to absorb the energy of reflected waves.

[7] In the present experiments, the spatial evolution of numerous realizations of a wavefield that all have identical initial frequency power spectra for the free wave components, but with random phases in each realization is studied. To generate the wavemaker driving signal for each realization, we start with a deterministic Gaussian-shaped unidirectional wave group, with the surface elevation variation in time given by

$$\eta(t) = \eta_0 \exp(-t/mT_0)^2 \cos(\omega_0 t), \tag{1}$$

where $\omega_0 = 2\pi f_0 = 2\pi/T_0$ is the carrier wave circular frequency, η_0 is the maximum wave amplitude in the group, and the parameter m defines the width of the group. The wave number k is related to ω by

$$\omega^2 = kg \tanh(kh). \tag{2}$$

The spectrum of (1) also has a Gaussian shape with the relative width at the energy level of half of the maximum that depends on the parameter m:

$$\Delta\omega/\omega_0 = \frac{1}{m\pi}\sqrt{\frac{\ln 2}{2}}. \tag{3}$$

The value of the spectral width parameter in the present experiments was selected to be m = 3.5, yielding a quite narrow spectrum with $\Delta\omega/\omega_0$ = 0.054. Note that the Fourier transform of (1) is real, i.e., all spectral components are in phase. The discrete frequency spectrum is calculated for the surface elevation variation in time given by (1) for $-1024\Delta t \leq t < 1024\Delta t$, where Δt = 0.025 s is the sampling interval at 40 Hz. The total duration of a single group is thus 51.2 s (2048 data points), and the frequency resolution of the spectrum Δf is better than 0.02 Hz.

[8] To study spatial evolution of the wavefield, it is desirable to follow its variation over distances containing as many dominant wavelengths λ_0 as possible. Since the length of the facility is fixed, the shortest carrier wave period T_0 was selected based on the frequency response of the hydraulically driven wavemaker. All experiments were carried out for a carrier wave of period T_0 = 1.5 s, corresponding to the wavelength λ_0 = 3.51 m and the dimensionless water depth $k_0h = 8.95 \gg 1$. Hence, in view of (3), the deep-water dispersion relation is satisfied for all significant harmonics in the spectrum. For the parameters chosen, the wavefield propagates along the tank with the group velocity c_g = 1.17 m/s.

[9] The spectrum of (1) was then truncated to leave 60 harmonics around the carrier frequency $f_0 = 1/T_0$ containing all components with nonnegligible amplitudes that can be faithfully excited by the wavemaker. For every realization of the surface elevation generated at the wavemaker, the amplitude of each spectral component a_i (i = 1, . . ., 60) is assigned a phase $\varphi_i = n\pi/256$, where n is a random integer, $-255 \leq n \leq 256$. To obtain the corresponding spectral component of the required wavemaker stroke, the linear transfer function for a piston-type wavemaker [see, e.g., *Dean and Dalrymple*, 1991] is applied. Minor empirical corrections for both the amplitudes and the phases of each stroke harmonic appropriate for the Hanover facility were introduced into the theoretically derived transfer function. The inverse Fourier transform of the resulting complex amplitude spectrum yields the wavemaker driving signal required to excite a 51.2-s-long realization of a random unidirectional wavefield. In view of the 200 s limit on the total continuous operation time of the wavemaker in the facility, this signal was actually repeated three times, yielding three nearly identical wave groups with the total extent of 153.6 s. To eliminate finite wavemaker displacements at the beginning and at the end of the wave excitation period, and thus the piston acceleration and velocity beyond the mechanically acceptable limits, windowing was used by multiplying the wavemaker driving voltages by $w_1(t) = 1 - \exp(-\alpha^2 t^2)$, α = 1.0 s^{-1} at the initial stages of excitation, when $0 \leq t < 4$ s, and by $w_2(t) = \exp[-\alpha^2(t - t_0)^2]$ when t_0 = 149.6 s at the final stages.

[10] The instantaneous water height is measured using 25 resistance type wave gauges, distributed along the tank and attached to the tank wall. The wave gauges are located at a distance of about 0.5 m from the wall. For technical reasons, the nearest wave gauge is placed at about 50 m from the wavemaker. To reduce contamination of the results by waves reflected from the far end of the tank, the last wave gauge in the present experiments was located at 214 m from the wavemaker, so that the tail of group passes through this sensor before the arrival of the reflected waves from the beach at the far end of the tank. Besides those gauges, additional wave height sensors attached to the wavemaker and placed on a bridge at the distance of 3.5 m from the wavemaker are available.

[11] The calibration of the wave gauges was done by filling the tank first to the depth of 6 m and then reducing the depth in steps of 0.5 m to 3.5 m, thus covering the range of surface elevations relative to the undisturbed value from −1.5 m to 1.0 m. The calibration curve for each wave gauge was obtained by best fit to the linear dependence. Due to the size of the facility, the calibration procedure takes a whole work day. The wave gauges were therefore calibrated only once for the experimental session that lasted about 2 weeks. It is estimated that the absolute error in the measured instantaneous surface elevation did not exceed a few millimeters.

[12] The output voltages of all wave gauges, as well as the wavemaker driving signal and the output of the wavemaker position potentiometer that provides information on the instantaneous wavemaker displacement were sampled at 40 Hz for the total sampling duration of 400 s, sufficient for the wavefield excited by the wavemaker to propagate beyond the most distant wave gauge.

[13] Each experimental run started only at a sufficient interval from the previous experiment when the water surface was quiescent and all remaining disturbances decayed totally. The reflected wave energy absorption system effectively eliminated the remaining long waves in the tank and enabled relatively short (about 15 min) intervals between consecutive experimental runs.

[14] The maximum possible for a deterministic wave group (1) wave steepness defined as $\varepsilon = \eta_0 k_0$ is adopted as the measure of nonlinearity of the wavefield. For deterministic wave groups, the distance at which nonlinearity effects become essential scales as ε^2 [*Shemer et al.*, 1998, 2002, 2007]. Higher values of ε therefore allow more prominent manifestation of the nonlinear effects along the tank. Visual observation of the wavefield during initial runs performed with $\varepsilon = 0.3$ showed occasional wave breaking within the tank. Since wave breaking is not accounted for in the deterministic models of wavefield evolution such as the equation of *Dysthe* [1979] or equation of *Zakharov* [1968], it was decided to run most experiments for $\varepsilon = 0.25$, for which no breaking was observed. In addition, to estimate the effect of nonlinearity on the wavefield evolution, some experimental runs were carried out for $\varepsilon = 0.2$.

[15] The limited access time to such a large-scale facility as GWK and the considerable duration of each experimental run restrict the number of realizations of a random wavefield that can be investigated experimentally. The total number of experimental runs in this study is 69 (10 for $\varepsilon = 0.2$, denoted as series A in sequel, 46 runs for $\varepsilon = 0.25$, series B, and 13 runs for $\varepsilon = 0.3$, series C).

3. General Definitions and Models of Probability Distributions Function

[16] In a unidirectional wavefield, the variation of the surface elevation $\eta(t)$ at any fixed distance x from the wavemaker can be written as

$$\eta(t) = \mathrm{Re}\left[\sum_{m=1}^{M} a_m \exp(i\omega_m t)\right], \tag{4}$$

where the complex amplitudes $a_{\mathrm{m}} = a\,(\omega_m, x)$ consist of a sum of free and bound waves:

$$a(\omega_{\mathrm{m}}, x) = a_1(\omega_{\mathrm{m}}, x) + \varepsilon a_2(\omega_{\mathrm{m}}, x) + \varepsilon^2 a_3(\omega_{\mathrm{m}}, x) + \ldots \tag{5}$$

[17] In any laboratory experiment, the free wave spectrum $a_1(\omega_{\mathrm{j}})$ contains a finite number of discrete harmonics

$$\omega_{\mathrm{j}}^{(1)} = \omega_{\min}, \omega_{\min} + \Delta\omega, \ldots, \omega_{\max}; \quad \omega_{\max} = \omega_{\min} + (N-1)\Delta\omega,\ j = 1, \ldots, N. \tag{6}$$

The frequency resolution of the spectrum $\Delta\omega$ is determined by the duration of the forcing signal T_{tot}, $\Delta\omega = 2\pi/T_{\mathrm{tot}}$. The wavenumbers of free waves obey the dispersion relation given by (2).

[18] The amplitudes of higher-order bound waves a_2 and a_3 at each location depend on the free wave amplitudes a_1. The wavenumbers and the phase velocity of these components depend on the parent free waves and cannot be determined using (2) [*Stiassnie and Shemer*, 1987].

[19] The amplitude of random waves is characterized by the standard deviation of the sea surface elevation, σ:

$$o^2 = \langle \eta^2 \rangle. \tag{7}$$

Note that (7) contains contributions of free and bound waves. The characteristic spectral frequency of the free waves, ω_m, the characteristic wave period, T_{m}, and the free wave spectral width, ν, are defined:

$$\omega_m = \frac{2\pi}{T_m} = \frac{m_1}{m_0}; \quad \nu = \sqrt{\frac{m_0 m_2}{m_1^2} - 1} \tag{8}$$

where

$$m_j = \int_{\omega_{\min}}^{\omega_{\max}} \omega^j S(\omega) d\omega \tag{9}$$

and $\omega_{\min} \le \omega \le \omega_{\max}$ defines the free wave frequency domain. For a Gaussian spectrum, the spectral width definitions (3) and (8) are related through $\Delta\omega/\omega_0 = \nu\sqrt{2\ln 2}$.

[20] As long as the free wave spectrum is sufficiently narrow, the frequency domains of the free and bound waves are separated. However, even for an initially narrow free wave spectrum, the widening in the course of evolution can lead to the overlapping frequency domains of free $\omega^{(1)}$ and bound waves $\omega^{(2)}$. Frequencies $\omega^{(2)}$, which result from the interaction of the free harmonics ω_{l} and ω_{m}, where l, $m = 1, \ldots, N$, can be subdivided into the second harmonics $\omega^{(2+)} = \omega_{\mathrm{l}} + \omega_{\mathrm{m}}$ and subharmonics $\omega^{(2-)} = \omega_{\mathrm{l}} - \omega_{\mathrm{m}}$. The second-order bound waves thus occupy the domains $\omega^{(2-)} < \omega_{\max} - \omega_{\min}$ and $2\omega_{\min} < \omega^{(2+)} < 2\omega_{\max}$. The frequency domains of third-order harmonics $\omega^{(3)}$ that have even smaller amplitudes can be defined using a similar approach.

[21] Spectrum widening can cause certain ambiguity in definition of the integration boundaries of the free-wave domain in (9). It appears, however, that the computed characteristic frequencies ω_m and spectral widths ν are quite

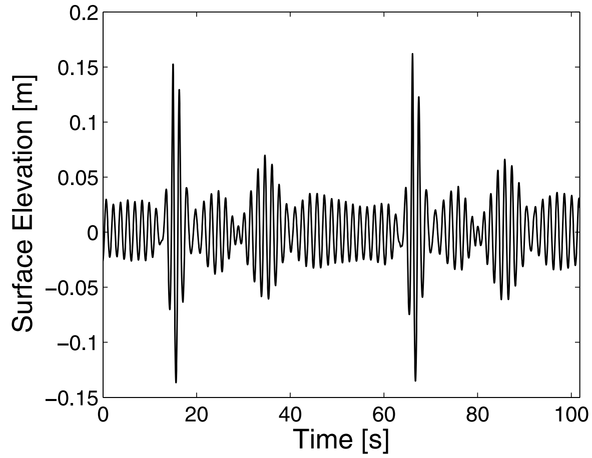

Figure 1. Measured wave sequence with two nearly identical extreme events (series B, x = 132 m).

robust and depend only weakly on the values of $\omega_{\min}$ and $\omega_{\max}$ selected.

4. Results

[22] The beginning and the end of the wave packet generated as described in section 2 are affected by the transient effects and the smoothing window applied on the wavemaker driving signal. To reduce the influence of the end effects on the data, at each fetch the midpoint, t_0, of the recorded wave packet was determined, and the data for -51.2 s $\leq t - t_0 \leq 51.2$ s, i.e., representing the duration of 102.4 s corresponding to two full periods of the driving signal and thus containing two practically identical wave groups, were considered. At each location, the mean value for each distance from the wavemaker and for each realization was subtracted before further processing. A typical appearance of extremely high waves is illustrated in Figure 1. This phenomenon repeats itself. Clearly, Figure 1 does in fact display two similar sequences of 2–3 waves considerably larger than the waves in the background.

[23] It is customary to characterize waves by the significant wave heights $H_{1/3}$ representing the average trough-to-crest height of 1/3 highest waves in each record [*Goda*, 2000]. Values of $H_{1/3}$ were calculated here by considering the wave records at each fetch and averaging over the ensemble for each experimental series. The variation of $H_{1/3}$ with the fetch presented in Figure 2 indicates that for each forcing amplitude, the significant wave height remains approximately constant. In spite of the presence of experimental errors within about ±0.5 cm that can be attributed to inaccuracies in the calibration of wave gauges, a certain systematic decrease in wave heights along the tank can be noticed. This effect is quite weak but seems to increase with the forcing amplitude, suggesting that sporadic wave breaking plays a dominant role in the wave energy dissipation.

[24] Alternatively, the amplitude of random waves can be characterized by the standard deviation of the sea surface elevation, σ, see (7). For linear narrowband waves with Rayleigh-distributed amplitudes, the following relations holds between the significant wave height $H_{1/3}$ and the root-mean-square of the surface elevation,

$$H_{1/3} = 4.004\ \sigma. \qquad (10)$$

[25] The spectral shape of free waves component at the wavemaker was prescribed to be Gaussian. The spatial evolution of the ensemble-averaged spectral density $S(f = \omega/2\pi)$ for the series B is shown in Figure 3. In the initial stages of evolution shown in Figure 3a, the spectral density widens around the carrier wave frequency f_0 = 0.67 Hz up to the distance of about 100 m, or 30 carrier wavelength λ_0. This is more pronounced at the high-frequency side. At the subsequent stages of the spatial evolution, presented in Figure 3b, the spectrum tends to its initial shape at a distance of about 200 m or 60 λ_0 from the wavemaker. The patterns of spatial evolution of the spectra at both lower (series A) and higher (series C) initial forcing amplitudes are similar, and also exhibit the effect of quasi-recurrence.

[26] The characteristic wave frequency ω_m remains nearly constant along the tank with the average value of ω_m = 4.21 rad·s^{-1} for the series A, ω_m = 4.20 rad·s^{-1} for series B and ω_m = 4.16 rad·s^{-1} for series C. The frequency limits $\omega_{\min}$ and $\omega_{\max}$ in (9) are defined by the first minima of $S(f)$ on both sides of the characteristic frequency $f_m = \omega_m/2\pi$. As shown in Figure 4, the spectral width ν varies notably along the tank and does not recover to its initial value fully. In the narrow spectra at x = 3.5 m ($x/\lambda_0 \approx 1$), and at x = 214 m ($x/\lambda_0 \approx 60$), the domain of free waves around f_0 is clearly separated from the second-order bound waves around $2f_0$, which in turn are quite distinguishable from the weaker third-order bound waves around $3f_0$. The widening of the free-wave spectrum around 100 m from the wavemaker causes even stronger widening of the bound-wave spectrum. As a result, the free-wave spectral widening around x/λ_0 = 30 smears the spectral boundaries between the free and bound waves, thus making it impossible to differentiate between the second- and the third-order bound-wave frequency domains.

[27] The variation along the tank of the spectral densities at frequencies close to $f_{\min}$ and $f_{\max}$ is shown in Figure 5 for

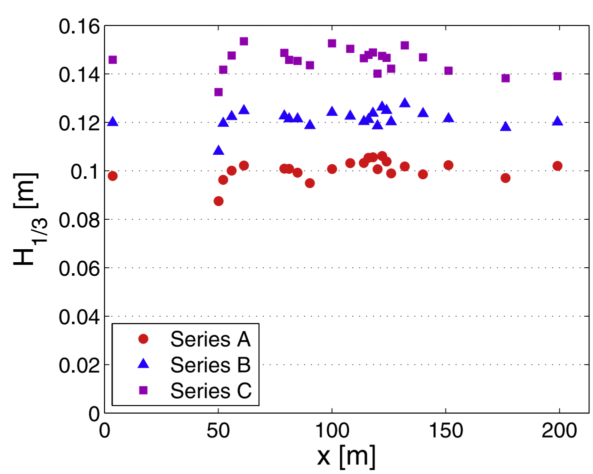

Figure 2. Variation of the measured significant wave height along the tank.

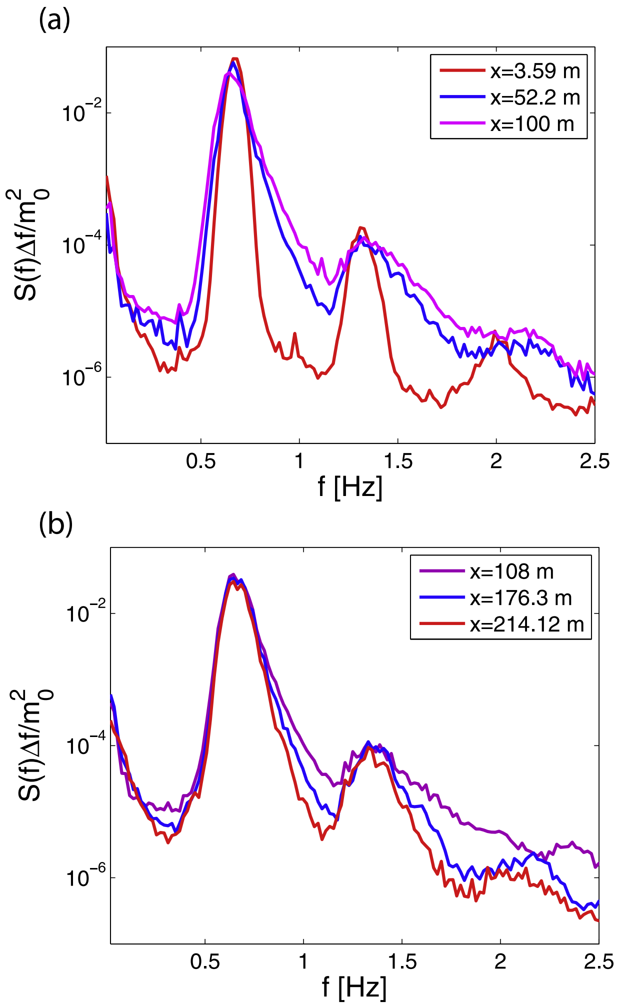

Figure 3. (a) Evolution of the frequency spectrum for series B: spectrum broadening during the initial stages of the evolution. (b) Evolution of the frequency spectrum for series B: partial relaxation to narrower spectrum farther away from the wavemaker.

all three forcing amplitudes. In all cases, these components attain a maximum at a certain distance from the wavemaker and then decrease strongly again. Note that at higher forcing amplitudes, the maximum is attained at shorter distances from the wavemaker.

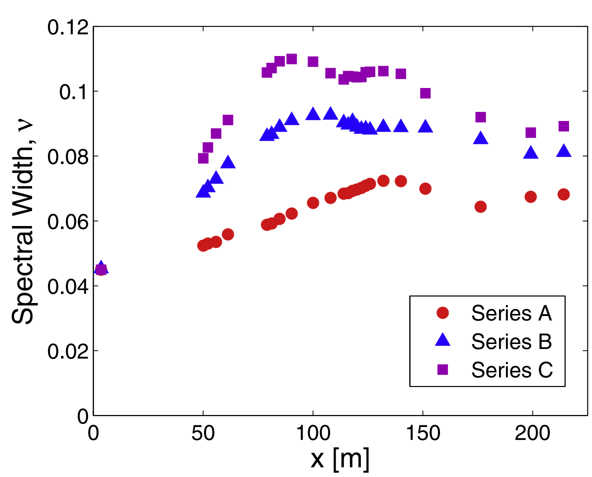

Figure 4. The variation of the spectral width along the tank.

[28] The skewness and the kurtosis coefficients of the surface elevation are defined, respectively, as

$$\lambda_3 = \frac{\langle \eta^3 \rangle}{\sigma^3}; \quad \lambda_4 = \frac{\langle \eta^4 \rangle}{\sigma^4}. \tag{11}$$

[29] For a normally distributed wavefield, $\lambda_3 = 0$ and $\lambda_4 = 3$. The variations of λ_3 and λ_4 along the tank are presented in Figure 6. In particular, Figure 6a demonstrates that for all conditions, the skewness λ_3 that characterizes the vertical asymmetry of surface elevation is positive and it increases with the nonlinearity of the wavefield. According to *Tayfun* [2006], the upper limit of the skewness coefficient in a narrowband wavefield was composed solely of second-order bound waves in deep water is

$$\lambda_3^{\mathrm{up}} = 3 m_0^{1/2} \omega_{\mathrm{m}}^2 / \mathrm{g}. \tag{12}$$

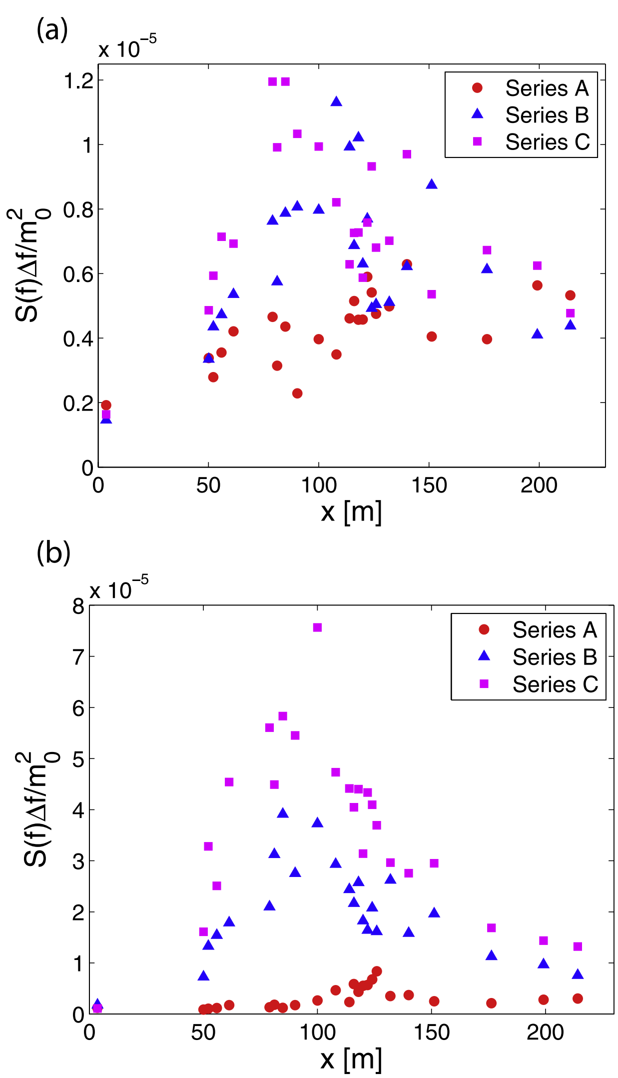

Figure 5. (a) Variation along the tank of the spectrum density at the frequency of f = 0.31 Hz. (b) Variation along the tank of the spectrum density at the frequency of f = 1.15 Hz.

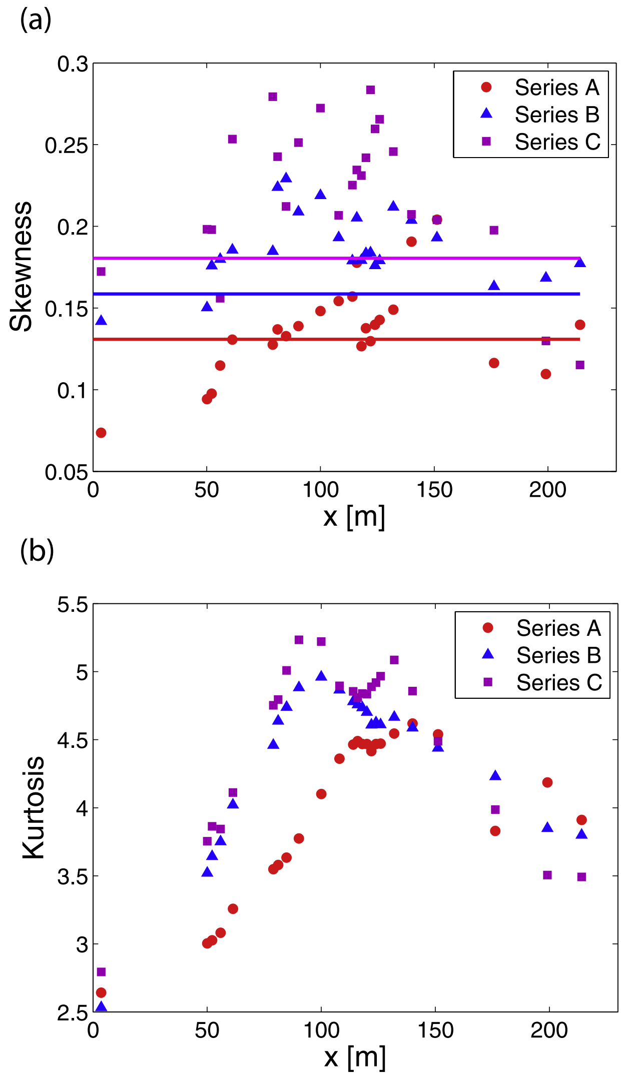

Figure 6. (a) Spatial evolution of the skewness. Solid denotes the upper limit of λ_3 according to *Tayfun* [2006]. (b) Spatial evolution of the kurtosis.

[30] As demonstrated in Figure 4, the values of the spectral width parameter ν are almost always below 0.1. So, the narrow spectrum approximation is valid for our experiments. The upper limits of λ_3 as given by (12) are also plotted in Figure 6a for all three experimental series and they clearly underestimate the measured values, except near the wavemaker where near-resonant free-wave interactions have not yet became effective. Note also that for every experimental series, the values of the coefficient λ_3 seem to increase first and decay farther away from the wavemaker. The kurtosis coefficient λ_4 in Figure 6b exceeds the value of 3 for all forcing amplitudes and at all distances x from the wavemaker, indicating a significant presence of large amplitude waves in the distribution. The values of λ_4 grow as the wave nonlinearity increases. Similarly to the skewness dependence on x, the variation of kurtosis with x is not monotonous, attaining a maximum at shorter distances from the wavemaker as the forcing amplitude is increased. A somewhat similar behavior of λ_4 was reported by *Mori et al.* [2007].

[31] Probability distribution functions are considered next. For linear narrow-band Gaussian waves, *Longuet-Higgins* [1952] demonstrated that the distributions of wave crest/trough heights A and of the wave heights H, scaled by σ, tend to follow the Rayleigh exceedance distributions

$$F(A) = \exp\left(-\frac{A^2}{2}\right), \tag{13a}$$

$$F(H) = \exp\left(-\frac{H^2}{8}\right). \tag{13b}$$

[32] *Longuet-Higgins* [1963] also has shown that nonlinearities can cause the statistics of surface elevations to deviate from the Gaussian statistics. Numerous laboratory experiments, in situ measurements and numerical simulations indeed support this conclusion [see, e.g., *Mori and Yasuda*, 2002; *Mori et al.*, 2007, and references therein]. The present results on the variations of higher-order moments

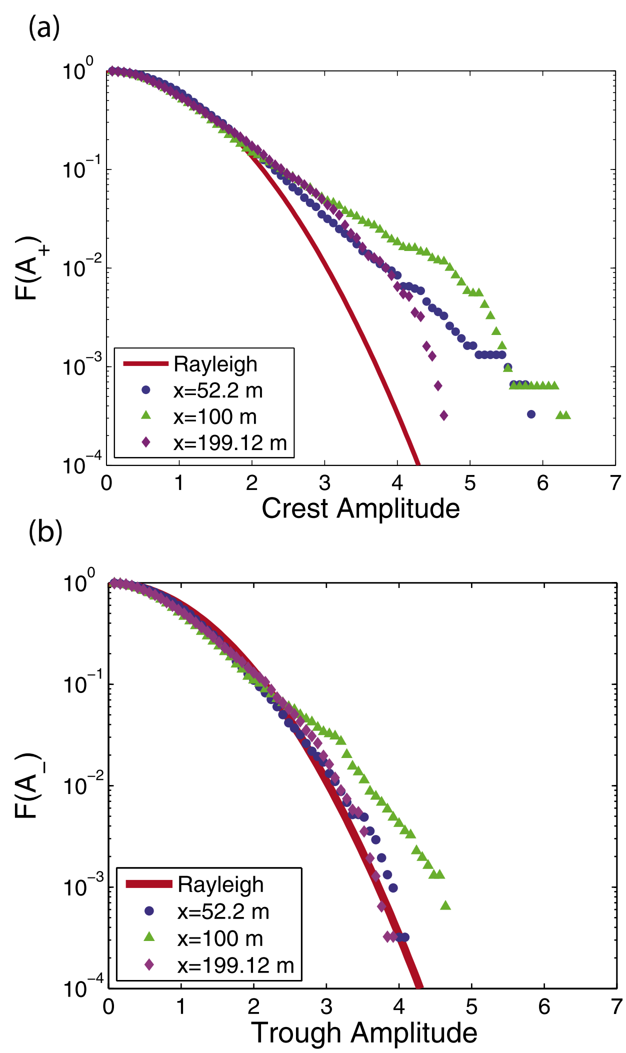

Figure 7. (a) Variation along the tank of the probability distribution functions of wave crest amplitudes, series B. (b) Variation along the tank of the probability distribution functions of wave trough amplitudes, series B.

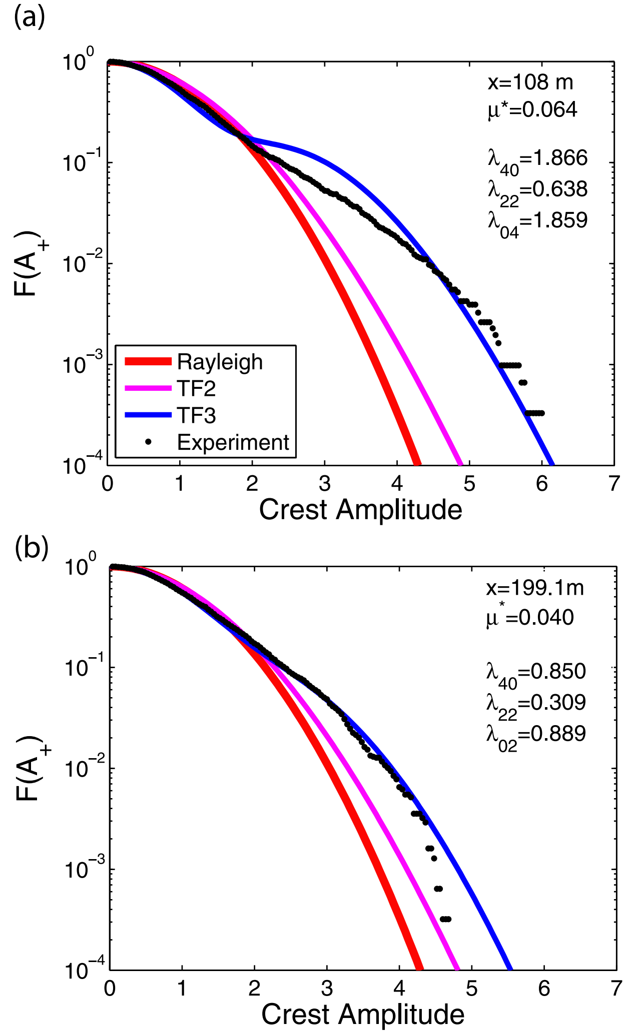

Figure 8. (a) Comparison of the experimentally measured wave crest amplitude distributions with the Rayleigh and the second (TF2)- and the third (TF2)-order Tayfun and Fedele distributions, series B, at x = 108 m. (b) Same as Figure 8a but for x = 199.1 m.

and cumulants of surface elevations along the tank also serve as a clear indication of deviations from the Rayleigh distribution and suggest that the extent of these deviations may vary with the distance from the wavemaker.

[33] The crest amplitude, say A_+, is calculated as a maximum of surface elevation between two zeros of the surface elevation, while the trough amplitude, A_-, is the minimum of surface elevation between two consecutive zeros. Both parameters are scaled by $m_0^{1/2}$. The crest-to-trough wave height, H, is defined as a sum of these two values.

[34] The qualitative similarities and quantitative differences in probability distribution functions for crest and trough amplitudes are demonstrated in Figure 7. The distributions are shown for three locations: relatively close to the wavemaker, at the distance corresponding to the maximum of the spectral width ν, and at the far end of the measuring domain. The distributions for both A_+ and A_- exhibit initial widening and then become narrower farther away from the wavemaker. For wave trough amplitudes, the distributions do not differ notably from the Rayleigh shape, except for the location with the maximum local spectral width at x = 100 m. Contrary to that, the wave crest amplitude probabilities exceed significantly the Rayleigh distribution. The difference in the behavior of crest and trough amplitudes is clearly related to the positive skewness as shown in Figure 6a.

[35] The accuracy of the second-order (marked as TF2) and the third-order (marked as TF3) estimates of distributions for the wave crest probabilities according to the model of *Tayfun and Fedele* [2007] is examined in Figure 8. The values of the statistical parameters used in computing TF2 and TF3 curves at each location are given in the corresponding figures, where λ_{40}, λ_{22}, λ_{04} are the fourth-order joint cumulants and μ* is a measure a surface slope or steepness [*Tayfun and Fedele*, 2007, equations (40) and (56)]. Figure 8 demonstrates that the second-order model distribution TF2 underestimates the deviations from the Rayleigh curve as compared to the experimentally measured dependencies. The higher-order TF3 distribution offers a much better description of the experimental results for the quite different spectral widths at both locations.

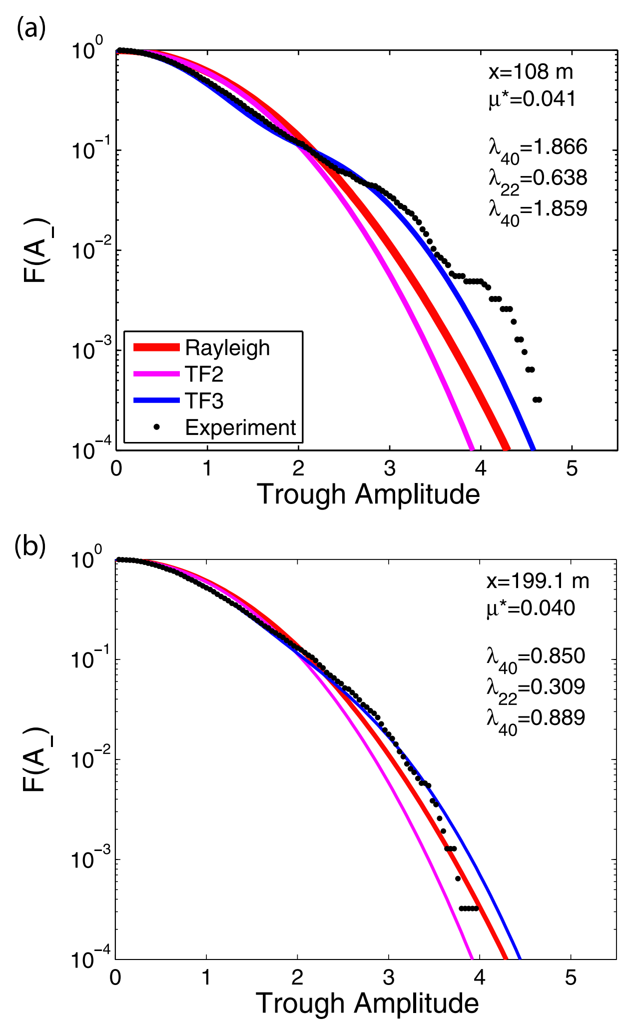

Figure 9. (a) Same as Figure 8a but for trough amplitudes. (b) Same as in Figure 8b but for trough amplitudes.

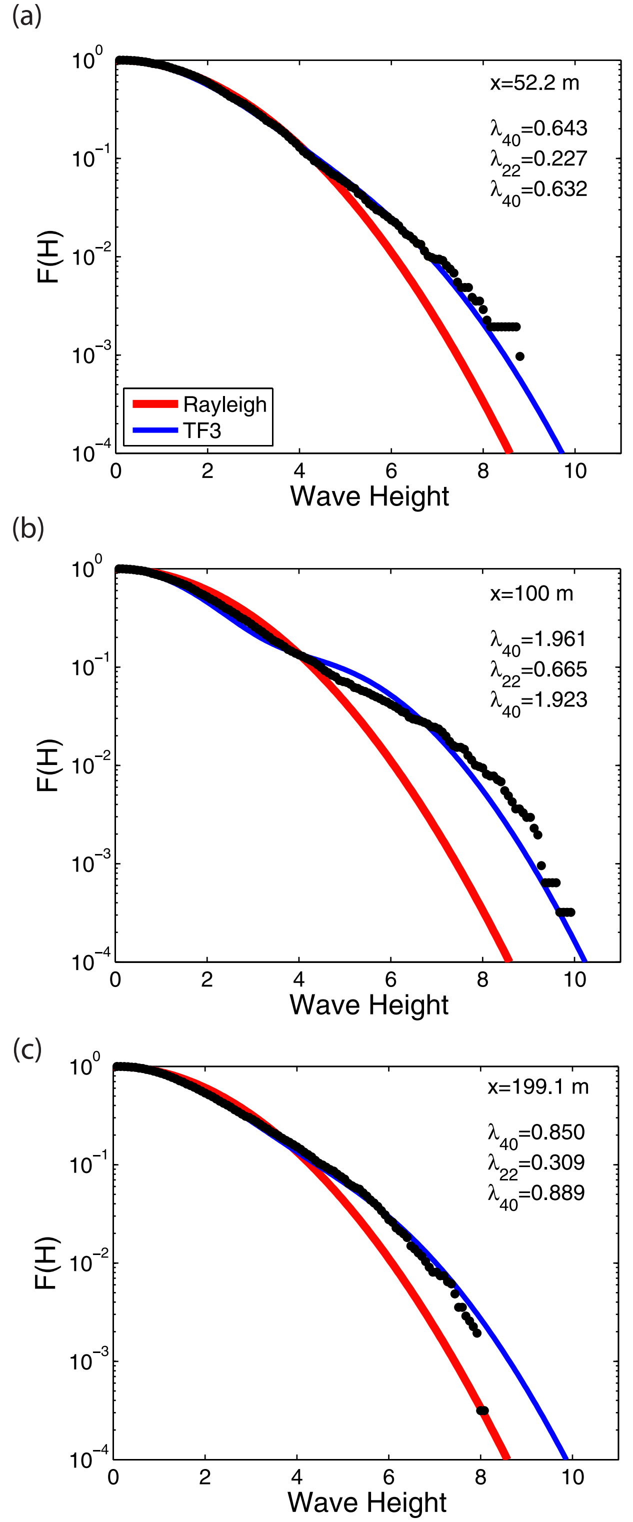

Figure 10. (a) Wave height probability distribution at x = 52.2 m, series B. (b) Same as Figure 10a but for x = 100 m. (c) Same as Figure 10a but for x = 199.1 m.

[36] An analysis of the accuracy of TF2 and TF3 distributions for the trough amplitudes is carried out in Figure 9. For low amplitudes ($A_- < 2$) both distributions reflect qualitatively correctly the lower (relative to the Rayleigh distribution) probabilities of trough amplitudes. For $A_- > 2$, both the measured values and the curves according to the TF3 model remain above the Rayleigh distribution, while the TF2 model strongly underpredicts the probability of higher trough amplitudes.

[37] Wave height probability distributions for the experimental series B are presented in Figure 10 and compared with the corresponding third-order TF3 curves. For low wave heights ($H < 5$) the distribution follows the Rayleigh shape at x = 52.2 m, Figure 10a. However, at larger distances from the wavemaker deviations from the Rayleigh distributions can be identified, see Figures 10b and 10c, with the measured probabilities being below the Rayleigh values. Note that the third-order TF3 distribution seems to describe this effect appropriately. For larger wave amplitudes, the deviations from the Rayleigh distribution exist at all locations, being more pronounced at x = 100 m, the distance that corresponds to the maximum of spectral width ν, as shown in Figure 10b. The TF3 distribution seems to remain valid for all locations along the tank, although the agreement of TF3 with experimental data in Figure 10b is somewhat less impressive.

[38] The effect of nonlinearity is studied in Figure 11. The wave height distributions are presented here for the lowest (series A) and highest (series C) values of the wave steepness ε. The distributions presented at distances corresponding to the maximum of the spectral width ν are compared in Figure 11 with the third-order theoretical curves TF3. The experimentally determined probability of very high waves exceeds predictions based on the Rayleigh distribution, with the deviation that increases with the nonlinear parameter ε. For low waves the dependence of the deviation from the Rayleigh distribution on ε is less pronounced. The TF3 curves are in a good agreement with the experiment.

5. Discussion

[39] The results of the previous section clearly demonstrate the variations of different wavefield parameters along the tank. While the total energy of the wavefield is approximately conserved, and the occasional breaking does not seem to cause significant dissipation (Figure 2), the spectral

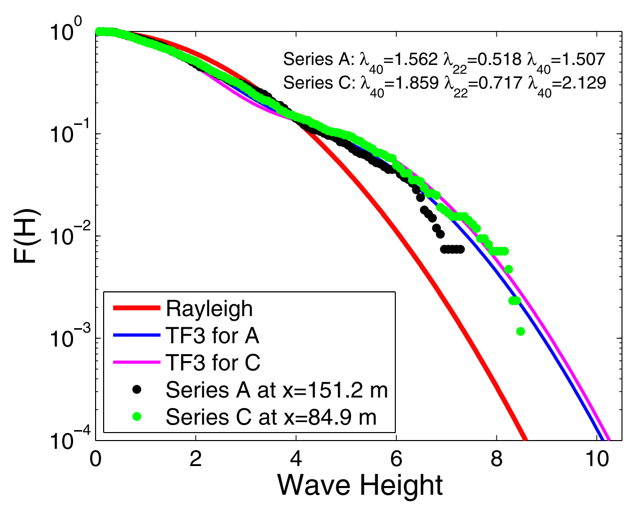

Figure 11. Wave height probability distributions for series A and C.

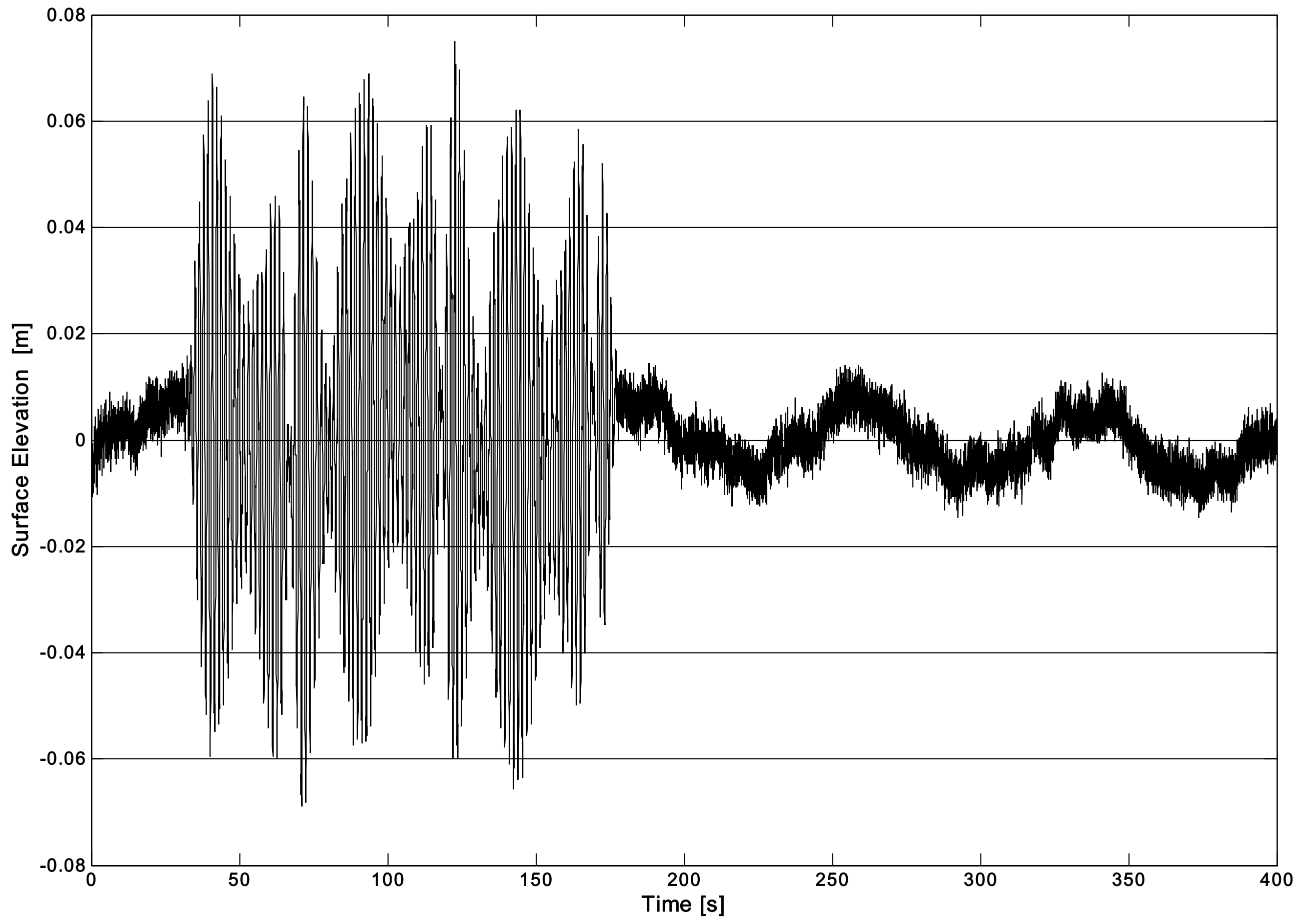

Figure 12. Example of recorded low-amplitude long wave that is clearly visible after wavemaker-excited short waves pass by the wave gauge at $x = 3.59$ m.

width undergoes noticeable variation in the evolution process. The initially narrow spectra become wider and attain maximum width at a certain distance from the wavemaker (see e.g., Figures 3, 4, and 5). The larger the nonlinearity of the wavefield, the more pronounced is the change in the spectral width and the shorter the distance where it attains a maximum. The present results suggest that the characteristic linear scale of the spatial evolution of the wavefield is proportional to ε^{-2}, as is the case for the evolution of deterministic nonlinear wave groups that is adequately described by the spatial versions of the equation of *Dysthe* [1979] for the narrow wave spectrum [*Shemer et al.*, 2002], or of the equation of *Zakharov* [1968] for an arbitrary initial spectral width [*Shemer et al.*, 2001, 2007].

[40] Other statistical wavefield parameters studied here also exhibit spatial variations strongly related to the local spectral width ν. For example, the kurtosis of the surface elevation attains a maximum at those locations where ν is large. Similarly, the tails of probability distribution functions of the wave heights, wave crests and wave troughs attain maximum deviation from the Rayleigh distribution at similar distances from the wavemaker. For locally wider spectra, considerable deviations from the Rayleigh shape are observed not only for the distribution tails, but also for low values of crest and trough amplitudes, as well as for low wave heights. It appears that the third-order model distributions presented by *Tayfun and Fedele* [2007] capture these phenomena adequately for the whole length of the tank and for all values of the nonlinear parameter ε.

[41] *Dysthe et al.* [2003] carried out numerical simulations of the temporal evolution of a narrow-banded random wavefield using the two-dimensional version of the Modified Nonlinear Schrödinger (MNLS) or Dysthe equation. They observed the widening of the wave number spectrum and its evolution to an asymmetric shape. These results are in general agreement with the present measurements. *Dysthe et al.* [2003], however, concluded that the wave number spectrum evolves relatively fast toward a quasi steady state. Such a quasi steady state is apparently not attained in our experiments. The wavefield in the present experiments was nearly perfectly unidirectional. This fact may constitute a possible reason for this qualitative difference in the long-term behavior between the two-dimensional wavefield simulated numerically by *Dysthe et al.* [2003] and the present measurements.

[42] However, the recent publication by *Stiassnie et al.* [2008] prompts us to suggest a plausible alternative reason for the spatial variation of the statistical parameters of the random wavefield. In this paper, the recurrence effect for the correlation function was discovered numerically in the framework of Albers's equation for narrow-banded random surface waves on deep water [*Alber*, 1978]. Alber's equation is a random counterpart of the nonlinear Schrödinger equation and it describes the temporal evolution of

the ensemble-averaged correlation function $K(t, \tau) = \langle \eta_i(t + \tau/2) \cdot \eta_i(t - \tau/2) \rangle$. It appears that in the presence of a small disturbance to the cross-correlation function, it undergoes periodic recurrence similar to the Fermi-Pasta-Ulam recurrence observed for the deterministic narrow wave groups in the framework of the nonlinear Schrödinger equation and obtained analytically for a three-wave system by *Shemer and Stiassnie* [1985] using the Zakharov equation. It is important to stress that *Stiassnie et al.* [2008] indicate that the recurrence period (or the recurrence length in the spatial evolution case) scales as ε^2, in agreement with the present observations and with the characteristic time scale in the computations of *Dysthe et al.* [2003]. In a subsequent paper, *Regev et al.* [2008] demonstrated that the instability of cross-correlation function is related to the inhomogeneity of the random wavefield. They have shown that interaction of a deterministic swell that serves as an inhomogeneous disturbance with a homogeneous narrow-banded random sea wavefield results in periodic recurrence on a long timescale.

[43] While the temporal wavefield excited at the wavemaker can be considered approximately stationary, the end effects related to the initiation and the end of the wavefield generation lead to the appearance of long shallow-water waves in the tank (seiche). This effect is known to exist in every laboratory wave channel. While long waves excited during the transient stages have different frequencies, the most persistent are usually those in resonance with the tank geometry, the so-called resonant sloshing waves. The tank depth of h = 5 m for those waves corresponds to shallow-water conditions so that their propagation velocity is $c = (gh)^{1/2}$ = 7 m/s. At larger distances from the wavemaker these waves tend to become more regular. Such waves with an apparent period of about 80 s can be attributed to the longest resonant sloshing mode with the length corresponding to twice the channel effective length, i.e., about 550 m. Their amplitude is less than 1 cm. These waves are indeed present in some realizations in our experiments, as demonstrated in Figure 12.

[44] The results of *Regev et al.* [2008] suggest that the recurrence period is of the order of hundred dominant wavelengths. This is in a qualitative agreement with the present results where the spectrum varies from its initial narrow shape to its widest form, the variation that can be seen as about half of the total recurrence period, at distances of about 30 to 40 dominant wavelengths.

[45] Two comments can be made with respect to the comparison of the numerical results of *Regev et al.* [2008] and of the present experiments in a wave tank. First, Alber's equation, which serves as the theoretical model in their numerical simulations, can be seen as a random counterpart of the nonlinear Schrödinger (NLS) equation. The NLS equation, however, proved to be inadequate as a quantitative model for prediction of evolution of deterministic wave groups [*Shemer et al.*, 1998, 2002; *Dysthe et al.*, 2003]. It is thus reasonable to assume that Alber's equation can at best describe only some general qualitative features of the evolution of a random wavefield. Second, the spatial extent of the present measurements does not cover even one full spatial recurrence period and thus does not allow to state definitely that spatial variations observed in the experiments can indeed be attributed to the recurrence as suggested by *Stiassnie et al.* [2008] and *Regev et al.* [2008]. It appears that additional numerical simulations of the spatial evolution of narrow-banded random wavefields with and without inhomogeneous disturbance carried out using advanced theoretical models and performed over extensive spatial domains are required to determine whether the significant variations of the statistical wavefield parameters observed in the present study can be related to the wavefield recurrence.

[46] **Acknowledgments.** The authors are indebted to K. Goulitski for his help in carrying out the experiments. We gratefully acknowledge the European community support under the Access to Research Infrastructures Action of the Human Potential Programme (contract HPRI-CT-2001-00157) that made possible experiments in the Large Wave Channel (G.W.K.) of the Coastal Research Center (F.Z.K.) in Hanover. The research is supported by grant 3-3573 from the Israel-Russia Cooperation Program; by grant 964/05 from the Israeli Science Foundation (L.S.); as well as by RFBR grants 06-05-72011, 08-02-00039, 08-05-00069, and INTAS 06-1000013-9236 (A.S.).

References

Alber, A. I. (1978), The effect of randomness on the stability of two-dimensional surface wavetrains, *Proc. R. Soc. London Ser. A*, *A363*, 525–546.

Annenkov, S. Y., and V. I. Shrira (2006a), Direct numerical simulation of downshift and inverse cascade for water wave turbulence, *Phys. Rev. Lett.*, *96*(20), 204501.

Annenkov, S. Y., and V. I. Shrira (2006b), Role of non-resonant interactions in the evolution of nonlinear random water wave fields, *J. Fluid Mech.*, *561*, 181–207.

Dean, R. G., and R. A. Dalrymple (1991), *Water Wave Mechanics for Engineers and Scientists*, 353 pp., World Sci., Singapore.

Dysthe, K. B. (1979), Note on a modification to the nonlinear Schrödinger equation for application to deep water waves, *Proc. R. Soc. London Ser. A*, *A369*, 105–114.

Dysthe, K. B., K. Trulsen, H. E. Krogstad, and H. Socquet-Juglard (2003), Evolution of a narrow-band spectrum of random surface waves, *J. Fluid Mech.*, *478*, 1–10.

Goda, Y. (2000), *Random Seas and Design of Maritime Structures*, 443 pp., World Sci., Singapore.

Hasselmann, K. (1962), On the nonlinear energy transfer in a gravity wave spectrum. part 1: General theory, *J. Fluid Mech.*, *12*, 481–500.

Longuet-Higgins, M. (1952), On the statistical distribution of the heights of sea waves, *J. Mar. Res.*, *11*, 245–266.

Longuet-Higgins, M. (1963), The effect of nonlinearities on statistical distributions in the theory of sea waves, *J. Fluid Mech.*, *17*, 459–480.

Mori, N., and T. Yasuda (2002), A weakly non-Gaussian model of wave height distribution for random wave train, *Ocean Eng.*, *29*, 1219–1231.

Mori, N., M. Onorato, P. A. E. M. Janssen, A. R. Osborne, and M. Serio (2007), On the extreme statistics of long-crested deep water waves: Theory and experiments, *J. Geophys. Res.*, *112*, C09011, doi:10.1029/2006JC004024.

Naess, A. (1985), On the distribution of crest-to-trough wave heights, *Ocean Eng.*, *12*, 221–234.

Onorato, M., A. R. Osborne, and M. Serio (2007), On the relation between two numerical methods for the computation of random gravity waves, *Eur. J. Mech. B Fluids*, *26*, 43–48.

Pelinovsky, E., and A. Sergeeva (2006), Numerical modeling of the KdV random wave field, *Eur. J. Mech. B Fluids*, *25*, 425–434.

Regev, A., Y. Agnon, M. Stiassnie, and O. Gramstad (2008), Sea-swell interaction as a mechanisms for the generation of freak waves, *Phys. Fluids*, *20*, 112102.

Shemer, L., and M. Stiassnie (1985), Initial instability and long-time evolution of Stokes waves, in *The Ocean Surface: Wave Breaking, Turbulent Mixing and Radio Probing*, edited by Y. Toba and H. Mitsuyasu, pp. 51–57, Springer, New York.

Shemer, L., E. Kit, H. Jiao, and O. Eitan (1998), Experiments on nonlinear wave groups in intermediate water depth, *J. Waterw. Port Coastal Ocean Eng.*, *124*, 320–327.

Shemer, L., H. Jiao, E. Kit, and Y. Agnon (2001), Evolution of a nonlinear wave field along a tank: Experiments and numerical simulations based on the spatial Zakharov equation, *J. Fluid Mech.*, *427*, 107–129.

Shemer, L., E. Kit, and H. Jiao (2002), An experimental and numerical study of the spatial evolution of unidirectional nonlinear water-wave groups, *Phys. Fluids A*, *14*(10), 3380–3390.

Shemer, L., K. Goulitski, and E. Kit (2007), Evolution of wide-spectrum wave groups in a tank: An experimental and numerical study, *Eur. J. Mech. B Fluids*, *26*, 193–219.
Stiassnie, M., and L. Shemer (1987), Energy computations for coupled evolution of class I and class II instabilities of Stokes waves, *J. Fluid Mech.*, *174*, 299–312.
Stiassnie, M., and L. Shemer (2005), On the interaction of four water-waves, *Wave Motion*, *41*, 307–328.
Stiassnie, M., A. Regev, and Y. Agnon (2008), Recurrent solutions of Alber's equation for random water-wave fields, *J. Fluid Mech.*, *598*, 245–266.
Tayfun, M. A. (1980), Narrow-band nonlinear sea waves, *J. Geophys. Res.*, *85*(C3), 1548–1552.
Tayfun, M. A. (2006), Statistics of nonlinear wave crests and groups, *Ocean Eng.*, *33*, 1589–1622.
Tayfun, M. A., and F. Fedele (2007), Wave height distributions and nonlinear effects, *Ocean Eng.*, *34*, 1631–1649.
Zakharov, V. E. (1968), Stability of periodic waves of finite amplitude on the surface of deep fluid, *J. Appl. Mech. Tech. Phys., Engl. Trans.*, *2*, 190–194.
Zakharov, V. (1999), Statistical theory of gravity and capillary waves on the surface of a finite-depth fluid, *Eur. J. Mech. B Fluids*, *18*, 327–344.

A. Sergeeva, Institute of Applied Physics, Russian Academy of Sciences, IAP RAS, 46, ul. Ulyanova, GSP–120, Nizhny Novgorod 603950, Russia.
L. Shemer, School of Mechanical Engineering, Faculty of Engineering, Tel-Aviv University, Tel-Aviv 69978, Israel. (shemer@eng.tau.ac.il)